Science Bulletin 66 (2021) 2320–2328

Contents lists available at ScienceDirect

Science Bulletin

journal homepage: www.elsevier.com/locate/scib

Article

Paleogeography control of Indian monsoon intensification and expansion at 41 Ma

Xiaomin Fang [a,b,*], Maodu Yan [a,b], Weilin Zhang [a,b], Junsheng Nie [c], Wenxia Han [d], Fuli Wu [a,b], Chunhui Song [e], Tao Zhang [e], Jinbo Zan [a,b], Yongpeng Yang [a,b]

[a] State Key Laboratory of Tibetan Plateau Earth System, Resources and Environment, Institute of Tibetan Plateau Research (TPESRE), Chinese Academy of Sciences, Beijing 100101, China
[b] Key Laboratory of Continental Collision and Plateau Uplift, Institute of Tibetan Plateau Research, Chinese Academy of Sciences, Beijing 100101, China
[c] Key Laboratory of Western China's Environments of Ministry of Education, Lanzhou University, Lanzhou 730000, China
[d] Shandong Provincial Key Laboratory of Water and Soil Conservation & Environmental Protection, School of Resource and Environmental Sciences, Linyi University, Linyi 276000, China
[e] School of Earth Sciences & Key Laboratory of Western China's Mineral Resources of Gansu Province, Lanzhou University, Lanzhou 730000, China

ARTICLE INFO

Article history:
Received 3 February 2021
Received in revised form 20 June 2021
Accepted 22 June 2021
Available online 21 July 2021

Keywords:
Asia paleogeography
Indian tropical monsoon
Eocene paleoenvironment
Subtropical monsoon onset
Driven factors and forcings

ABSTRACT

As a crucial part of the Asian monsoon stretching from tropical India to temperate East Asia, the Indian monsoon (IM) contributes predominant precipitation over Asian continent. However, our understanding of IM's onset, development and the underlying driving mechanisms is limited. Increasing evidence indicates that the IM began in the Eocene or even the Paleocene and was unexceptionally linked to the early rise of the Tibetan Plateau (TP). These were challenged by the heterogeneous and diachronous uplift of the TP and all the reported records were confined to tropical zone under tropical monsoon driven by the Intertropical Convergence Zone (ITCZ) that is irrelevant to the TP. Therefore, reliable paleoclimatic records from the extra-tropical IM region is crucial to reveal how the tropical IM expanded to subtropical and temperate zones and what driving factors might be related to it. Here we present robust Eocene paleoenvironmental records from central Yunnan (~26°N) in subtropical East Asia. The multiproxy results of two sites demonstrate a consistent sudden switch from a dry environment in the early Eocene to a seasonally wet one at 41 Ma, suggesting a jump of the tropical IM to the southern subtropical zone at 41 Ma. The full collision of India with Asia, and the resulting changes in paleogeography at 41 Ma (closure of the Neotethys sea, retreat of the Paratethys seas, fast northward movement of the southern margin of the TP and rise of the central TP), aided by synchronous Antarctic cooling, might have worked together to drive the IM enhancement and northward expansion.

1. Introduction

The Asian monsoon consists of Indian monsoon (IM) and East Asia monsoon (EAM). It stretches from the tropical Indian Ocean, South and Southeast Asia, and subtropical and temperate East Asia, to Northeast Asia at ~55°N and is the only exception from the encircled global tropical monsoon system confined to low latitudes (<20°–23°N and S). Modern observation and numerical modeling demonstrate that the global tropical monsoon is driven by the seasonal migration of the Intertropical Convergence Zone (ITCZ) [1,2] and irrelated to the uplift of the Tibetan Plateau (TP) (Fig. 1a, b) [4–6]. The studies and our recent data indicate that most moisture of the EAM region comes also from the IM [2,7] (Fig. 1c). Thus, the IM could play a critical role in the Asian monsoon system under which over half of the world's population lives. However, when the IM commenced and how it developed through time remain incompletely known and is still a subject of debate, which have hampered our understanding and prediction of the future Asian monsoon change with global warming.

The IM was previously thought to initiate in the late Miocene [8,9], or the early Miocene [10]; however, several recent studies greatly extended the initiation time back to the Eocene, the Paleocene [11–20] or even to the Cretaceous [11,21]. These large controversies arose mostly from undistinguishing of the IM and EAM from the more ancient ITCZ-driven tropical monsoon and from lacking of precisely dated continuous robust paleoclimatic records. Most reported Eocene or Paleocene IM records were actually within the range of the ITCZ-driven tropical monsoon. Poorly constrained geological evidence, because of lack of precise dating and

* Corresponding author.
E-mail address: fangxm@itpcas.ac.cn (X. Fang).

https://doi.org/10.1016/j.scib.2021.07.023

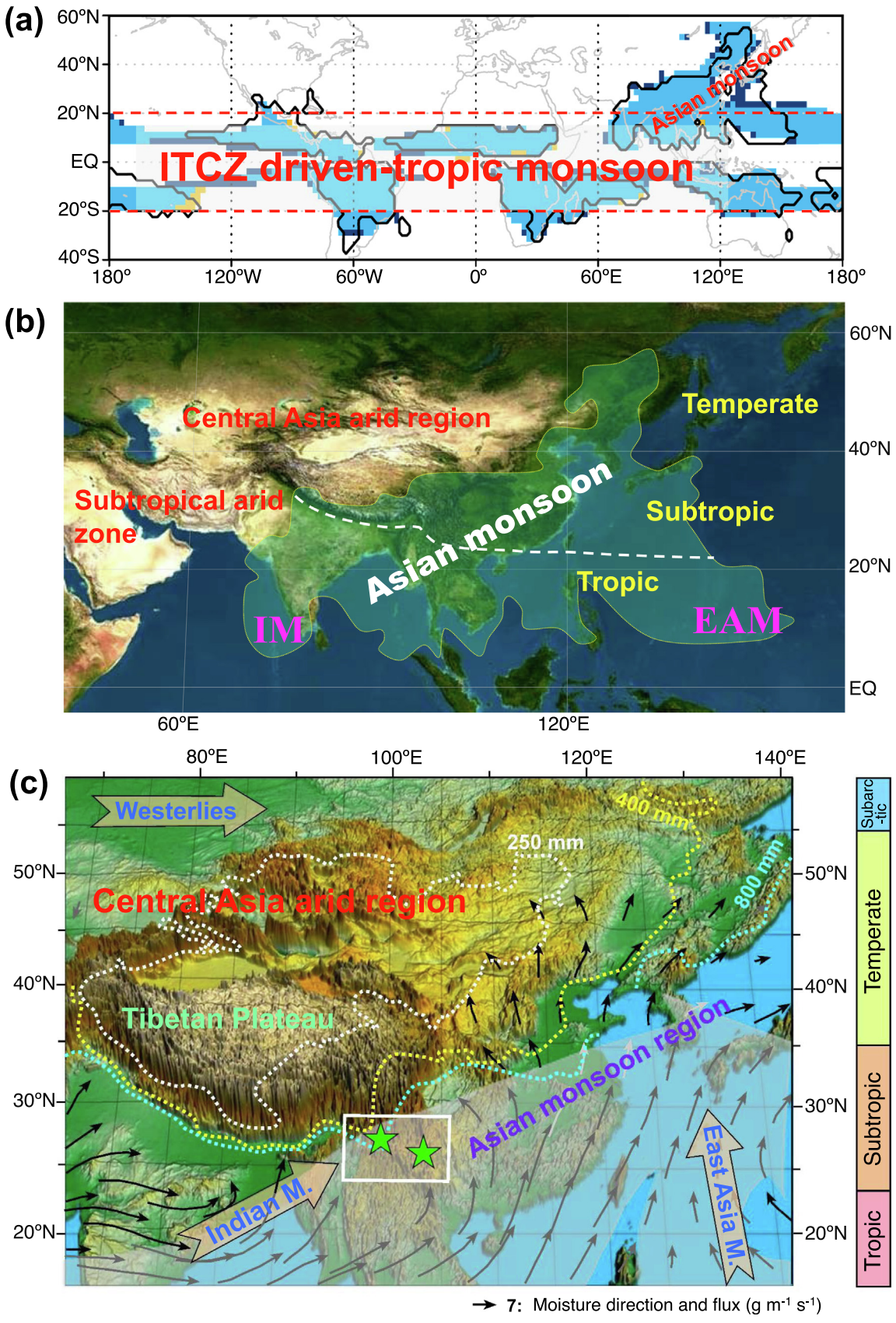
(a)
60°N
40°N
20°N
EQ
20°S
40°S
180°
120°W
60°W
0°
60°E
120°E
180°
ITCZ driven-tropic monsoon
Asian monsoon
(b)
Central Asia arid region
Temperate
Subtropical arid zone
Asian monsoon
Subtropic
Tropic
IM
EAM
60°N
40°N
20°N
EQ
60°E
120°E
(c)
80°E
100°E
120°E
140°E
Westerlies
400 mm
250 mm
800 mm
50°N
Central Asia arid region
40°N
Tibetan Plateau
30°N
Asian monsoon region
Indian M.
East Asia M.
20°N
Subarc-tic
Temperate
Subtropic
Tropic
7: Moisture direction and flux (g m-1 s-1)

reliable monsoon proxy, biases our precise understanding of the IM evolution.

Numerical modeling showed that without the TP, the IM was still over the Indian subcontinent and was confined <20°N as an ITCZ-driven tropical monsoon, but with the existence of the TP, the tropical IM jumped beyond the tropics northwards to the middle-latitude temperate zones [4–6], which here we named as the "extra-tropics" to distinguish the latitudinal positions from climate categorizations. Thus, long well-dated paleoclimatic records from the subtropical IM region are crucial to provide age constraints on northward expansion of the IM, because such area would have had dry climate due to the sinking air of the Hadley cell, and timing of seasonal climate wetting of this subtropical IM region would provide the best evidence for northward jump of the IM [22].

Here we provide well-dated robust continuous paleoenvironmental records from two 500-km apart parallel sections in Yunnan, SW China under the modern IM climate (Figs. 1c and S1–S3 online). Our records demonstrate that the IM has dramatically enhanced and expanded outside the tropics to the subtropical southern East Asia of ~26°N at 41 Ma.

2. Stratigraphy and chronology

2.1. Stratigraphy

Paleogene stratigraphy in Yunnan is widely distributed in many large long-narrow Meso-Cenozoic basins distributed between or along large transpressional faults, with basin surfaces at altitudes of ~1000–1500 m. Most Neogene and Quaternary sediments deposited in smaller narrow pull-apart basins in former larger Paleogene basins along slip faults and unconformably superimposed on the Paleogene stratigraphy. The unconformity represents a strong compression, uplift and erosion event in response to the continued indention of India into Asia (Fig. S1 online). These two suits of Cenozoic stratigraphy in Yunnan have long been recognized for their distinct characteristics. The lower part of the succession is represented by Paleogene red beds consisting of mostly purple-brown red fine conglomerates, sandstones and mudstones that contain evaporites (salts and gypsum) and eolian dune sandstones in some successions, while the upper part is formed of Neogene-Quaternary light coloured (grayish, greenish, yellowish) and coal-/limestone-bearing sediments [23]. The sharp lithological change has long been regarded as the evidence for the onset of Asian monsoon in the early Miocene [22]. Recent studies revealed that some previously regarded Neogene sediments are now dated to be the late Eocene and Oligocene in age [24–26]. We chose two 500-km apart parallel sections, the Shuanghe (SH) (103°57′19.4″E, 25°24′16.7″N) and Caijiachong (CJC) (99°50′40.1″E, 26°35′45.2″N) sections in the Yunnan Plateau with a mean altitude of ~1800–2000 m (Fig. 1c) for detailed chronological and monsoonal climate re-evaluation study.

The measured SH (300 m) and CJC (162 m outcrop + 90 m borehole = 252 m) sections from the two basins developed similar stratigraphic successions and lithology, with gypsum-bearing red beds in the lower and limestone/marl or/and coal-bearing sediments in the upper parts, indicating a sedimentary environment shift from a floodplain dominated environment to a swamp-fluviolacustrine succession, where evaporation mostly exceeds precipitation in the former but opposite in the latter (Figs. 2a, o, S2, and S3 online). The low but linear co-variance of limestone oxygen and carbon isotopes indicates that the upper parts of the SH and CJC sections were formed in fresh water closed lakes rather than in marine environments [28] (Fig. S4 online). This is further confirmed by the presence of fossil fresh water fish, crocodiles, gastropods and charophytes in the limestone/marl layers of the upper CJC section (Figs. 2 and S3 online). We have not observed any obvious erosion surface, instead a horizontal contact between the dry red beds and the above wet swamp-fluviolacustrine succession (Figs. S2 and S3 online). Thick volcanic rock layers are found in both sections, including three layers in the upper SH section and one 5-m thick tuff layer at the top of the CJC section (Figs. 2a, o, S2, and S3 online). These volcanic rocks show distinguishable characteristics of weathered soft lithology of grey color, pored and massive structure, and porphyritic texture with clearly visible phenocrysts of muscovite and biotite (Figs. 2a, o, S2, and S3 online).

2.2. Chronology

Laser U-Pb dating was applied to zircon grains from the uppermost volcanic layer imbedded in coal seams at thickness of 245 m of the SH section and the tuff layer at the top of the CJC section (Figs. 2a, o, S2, and S3 online). All the zircon grains show euhedral crystals with concentric rings indicative of magmatic origin and have similar ages with one distinct peak, yielding an average age of 37.03 ± 0.36 Ma (2σ) for the uppermost volcanic layer in the SH section and an average age of 35.49 ± 0.78 Ma (2 σ) for the tuff layer at the top of the CJC section (Fig. 3).

Slightly below this tuff layer presents the famous Caijiachong fauna, which was known as late Eocene in age and forest type fossil mammals [29,30] (Figs. 2o and S3 online), well agreed to our zircon U-Pb ages.

Detailed paleomagnetic analyses were applied to the two sections. Oriented samples were collected at intervals of 0.5–1 m. Rock magnetic measurements of some representative samples indicate that hematite and/or magnetite are the principle magnetic minerals (Fig. S5 online). Thermal demagnetization (TD) was performed for characteristic remanent magnetization (ChRM) isolation (Fig. S6 online). Positive reversals tests (Fig. S7 online) suggest that the secondary overprints of the ChRM were most likely cleaned. All reliable outcrop ChRM directions were turned into virtual geomagnetic pole (VGP) latitudes according to their declinations and inclinations, whereas the borehole ones are only inclinations, and both were plotted as function of depth in Fig. 2.

Fig. 1. Distribution of the Asian monsoon and location of the studied region. (a) Observed (thick contour) and simulated (shading) global monsoon domain showing an exceptional extension of the Asian monsoon from tropics up to the middle latitude of ~55°N in East Asia (modified from Ref. [2]). (b) The Asian monsoon range (taken from (a)) with respect to the TP and Asian inland and subtropical dry regions. (c) DEM showing the locations of the studied region (white square) and the SH and CJC sections (marked by green stars) with respect to the TP and the Asian monsoons. In (b), the white broken line shows the boundary between modern tropical and subtropical monsoons (taken from Ref. [1]). IM and EAM mean the Indian monsoon and East Asia monsoon, respectively. In (c), the white, yellow and light blue dotted lines indicate 250, 400 and 800 mm isopleths of mean annual precipitation, which divide the arid, semi-arid, sub-humid and humid monsoonal regions to their northwest and southeast, respectively. The solid arrows indicate moisture direction and flux (g/(m s)) at mean 850 hPa calculated from re-analyzed data of NOAA-CIRES in 1851–2014 by Dabang Jiang at the Institute of Atmospheric Physics, Chinese Academy of Sciences. Similar moisture paths of monsoons as grey shaded zones by Johnson [3] are also plotted for comparison. M. is the abbreviation of monsoon.

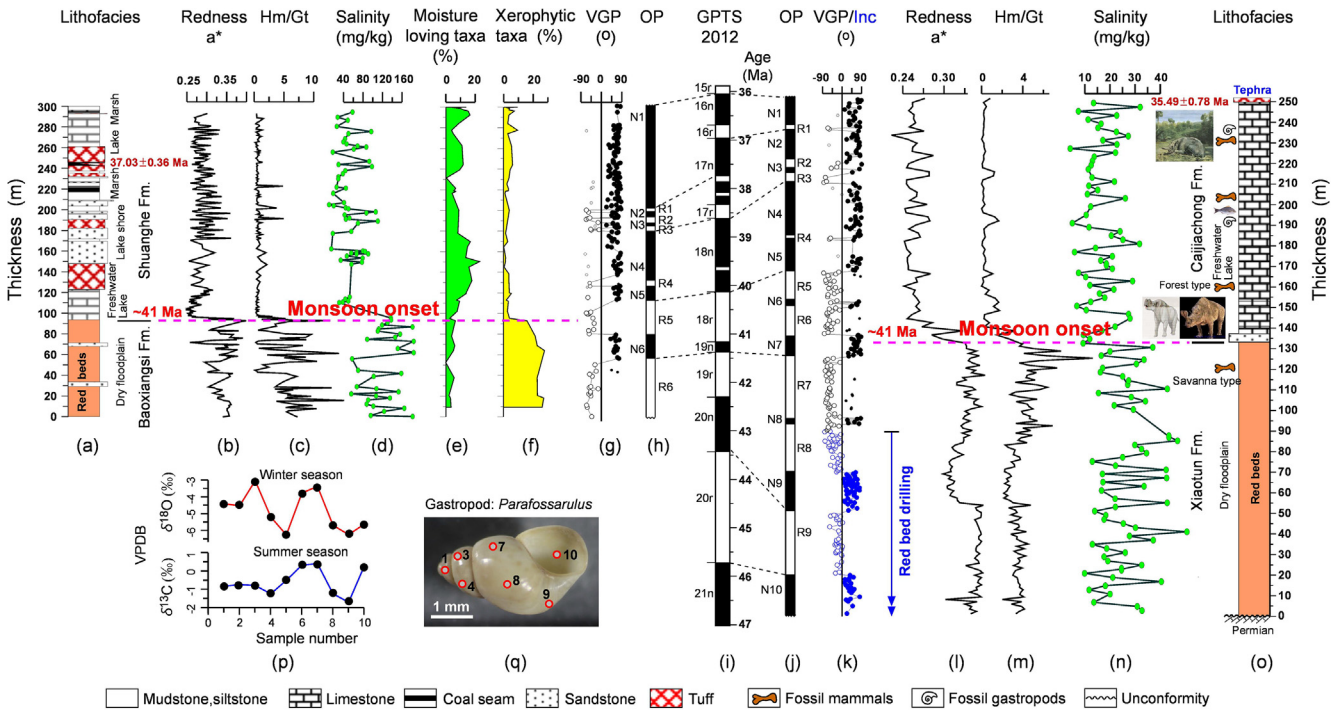

Fig. 2. Litho- and magneto-stratigraphy with lithofacies and climatic proxy records of sporopollen, redness, hematite/goethite (Hm/Gt) ratio and salinity as a function of depth for the SH (a–h) and CJC sections (j–o). Oxygen isotope variation along growth lines of a fossil gastropod *Parafossarulus* at the ~190 m level of the CJC section is shown in the lower-left part (p, q). The correlations of the observed magnetic polarities with the geomagnetic polarity time scale (GPTS) [27] chrons 16n to 19r for the SH section (g–i) and 16n–21n for the CJS section (i–k) are based on constraints of radiometric and fossil mammal ages in both sections (a, o and Figs. S2 and S3 online). Moisture-loving taxa refer to *Podocarpidites + Keteleeriaepollenites + Taxodiaceae* and xerophytic taxa are *Ephedripites + Chenopodipollis*. Note that the striking lithological changes from gypsiferous-calcareous red beds to freshwater limestones/marls in both sections and coal-bearing sediments in the SH section; the seasonal oxygen isotope variations in the gastropod shells from the upper CJC section (<41 Ma) and coincidental shifts of all environmental and climatic proxy records at ~41 Ma. All these collectively indicate the onset of the IM in Yunnan subtropical region at ~41 Ma. N and R in (h) and (j) are the observed normal and reversed polarities, respectively. Detailed stratigraphy, lithofacies and paleomagnetism are referred to Supplementary materials.

A total of 6 (10) normal and 6 (9) reversed polarity zones were obtained for the SH (CJC) section.

Utilizing the above two radiometric ages as the anchor points, the obtained magnetic polarity zones were well correlated to the chrons 16n to 19r for the SH section (i.e., N1–N5 to chrons 16n–18n, N6 to 19n, and R5–R6 to 18r–19r) and to 16n–21n for the CJC section (i.e., N1–N5 to chrons 16n–18n, N7, N9 and N10 to 19n, 20n and 21n, respectively) of the geomagnetic polarity time scale (GPTS) [27]. These correlations yield magnetostratigraphic ages of ~42.7–36 and ~47–36 Ma for the SH and CJC sections, respectively (Fig. 2) (see Supplementary materials for details). The abrupt lithofacies change from the lower red beds to the upper freshwater limestone/marl or coal series in both sections were thus constrained to be ~41 Ma (Fig. 2).

3. Evidence for a dry to wet transition and onset of the Eocene subtropical Indian monsoon

Paleoclimate records in these two sites consistently show a sharp dry-wet transition at 41 Ma (Fig. 2). This inference was based on several lines of evidence.

First, sediments change from red beds to limestones/marls in both sites at 41 Ma, interpreted as a result of lake expansion and climatic wetting (Figs. 2a, o and S2–S4 online). This sharp environmental change can be also seen clearly from sediment colour and hematite/goethite (Hm/Gt) ratio variations. Before 41 Ma, sediment redness and Hm/Gt ratio were high, but decreased rapidly at 41 Ma (Fig. 2c, m). It is well known that fine-grained hematite is a pigment and its high content indicates a dry climate [31,32]. Further evidence comes from decreased salinity, consistent with lake expansion and climatic wetting (Fig. 2d, n).

Second, the sporopollen record in the SH section provides further evidence. It shows that the vegetation was dominated by tropical-subtropical species (sparse forest-grassland of largely xerophilous plants such as Ephedra and Chenopodiaceae, and some broad-leaved tree species such as Carya, Castanea and Ulmus (chestnut, oak and elm)) before ~41 Ma but changed to the subtropical evergreen- and deciduous-broadleaved and coniferous tree mixed forest of mainly walnut, birch, pine, and spruce in the upper section after 41 Ma (Figs. 2e, f and S8 online). This shift is further indicated clearly by the rapid decrease of content of drought-tolerant plants of mostly Ephedra and Chenopodiaceae (from average 23.6% to 3.4%) and considerable increase of moisture-loving types from average 4% to 10.3% at ~41 Ma (Fig. 2e, f). Both suggest that the previous tropical-subtropical hot-dry climate was replaced by a subtropical warm-humid one at ~41 Ma.

Third, presence of fossils of freshwater fish, crocodiles, algae, gastropods and Charophytes and large mammals in the upper CJC section and few fossil rodents in the lower CJC section indicate a savanna-to-forest ecological environment shift at ~41 Ma, clearly suggesting climatic wetting (Figs. 2o and S3 online).

Fourth, stable isotope analyses indicate a seasonal wetting climate after 41 Ma in Yunnan. The oxygen isotope compositions of shell laminae along growth lines in the Assimineidae gastropod *Parafossarulus*, in the strata after 41 Ma, show significant seasonal variations, with peak values (~−7‰) similar to present day oxygen isotope values of stalagmites and lake carbonates in Yunnan [33,34]. Their mean value (~−5‰) is also similar to modern shells of gastropods and bivalves in Yunnan [35] (Figs. 2p, q and S4 online), suggesting a similar climate and strong IM during the late Eocene.

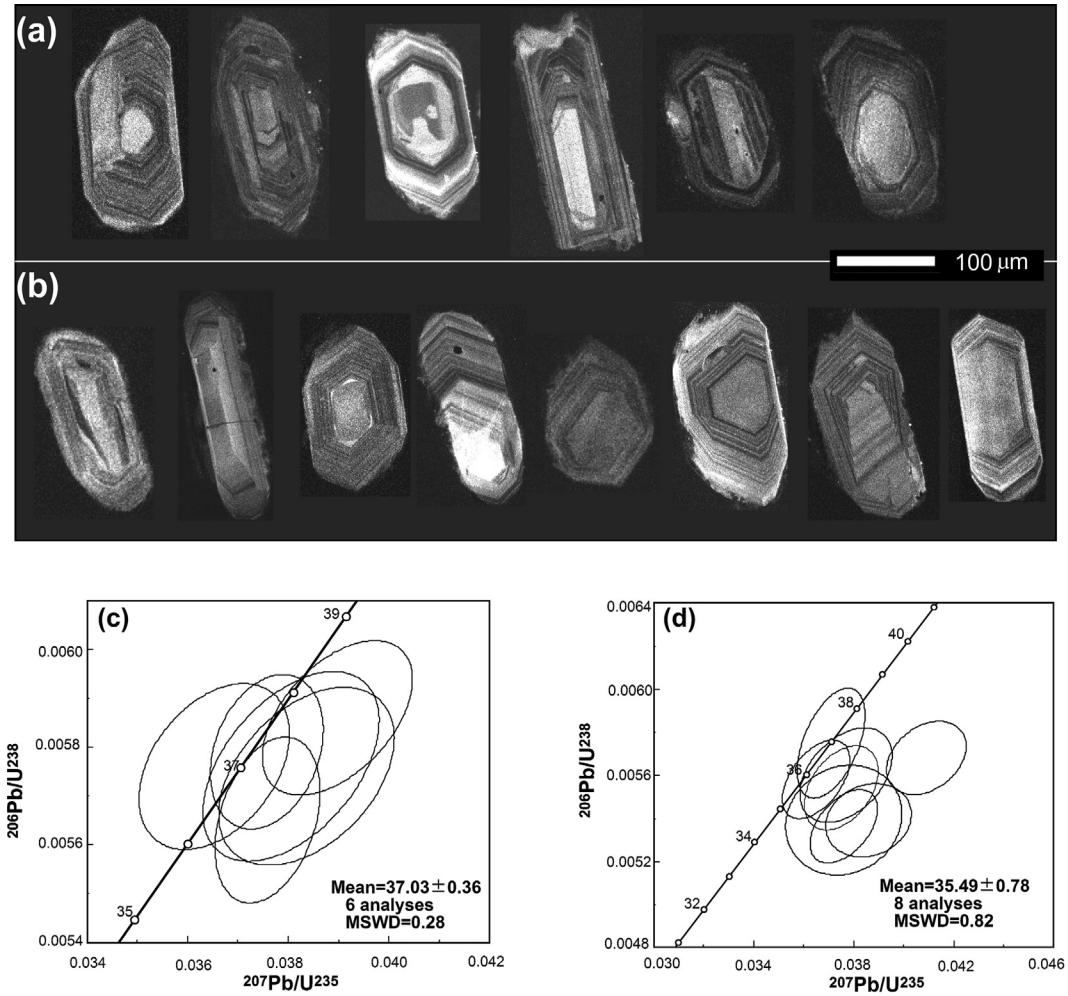

Fig. 3. Cathodoluminescence images of representative zircon grains (upper) and their concordia diagrams of LA-U-Pb dating (lower) for the tuffs in the SH (a, c) and CJC sections (b, d).

We interpreted the above shift of the paleoclimate and paleoenvironment from a dry-hot condition to a seasonal wet-warm one in Yunnan as a result of onset of the IM in the southern subtropics at 41 Ma associated with the IM enhancement and northward expansion.

4. Driving forcings for the IM intensification at 41 Ma

We notice that the IM intensification and expansion at 41 Ma is synchronous with full merging of the India-Asia continents, which we argue as the forcing for the observed IM intensification and expansion.

We argued that the remarkable decrease and rotation of the northward movement of the Indian plate at ~41 Ma following the India-Asia initial collision at ~55 ± 5/10 Ma [36–38] (Fig. 4b) could be a consequence of the full emerging of the Indian and Asian continents due to strong resistance from the Asian continent (Fig. 4a–c). This inference is also supported not only by the synchronous close of the Neotethys sea between the Indian and Asian continents [38] and fast retreat of the Paratethys sea to the northern side of the TP [39,40] (Figs. 4a–d and S9 online), but also synchronous cessation of the Gangdese magmatism (granitoid batholith intrusion and basaltic-andesitic volcanism) related to the Neotethyan oceanic slab subduction due to the successive subduction of the Indian continent [36,54–56]. Full merging of the India-Asia continents could have intensified the IM from several aspects which we elaborate as follows.

First, we suggest that the demise of the Neotethys sea [38] and a fast retreat of the Paratethys sea at ~41 Ma [39,40] (Figs. 4a–d and S9 online), which might be enhanced by the long-term Eocene global sea level decline trend [44,45] (Fig. 4d), might potentially cause the observed paleoclimatic and paleoenvironmental transition and intensification of the IM via two processes. (1) Neotethys sea disappearance can decrease the buffering ability of waterbody to temperature and precipitation variations in the IM region, intensifying the IM. This mechanism is similar to the proposed mechanism for the Paratetheys sea to account for the 30 Ma environmental changes [55]. However, the fast retreat of the Paratethys sea actually commenced at ~41 Ma rather than 30 Ma [39,40]. (2) Land area enlargement can increase land heating, especially in the tropical region, thus strengthening the Indian low-pressure center in summer, which is the key factor in determining the IM intensity in modern condition and model simulations.

Second, the full merging of the India-Asia continents would have caused widespread upper crustal deformation and uplift of the Gangdese Shan. Although an Andean-type Gangdese Shan at similiar to present elevation might have already existed during the Cretaceous and Paleocene [15], the Gangdese Shan had increased crust thickening and magnetism at ~50–51 Ma, probably due to break-off of the subducted Tethys oceanic slab from the Indian continent plate and basaltic underplating. This crust

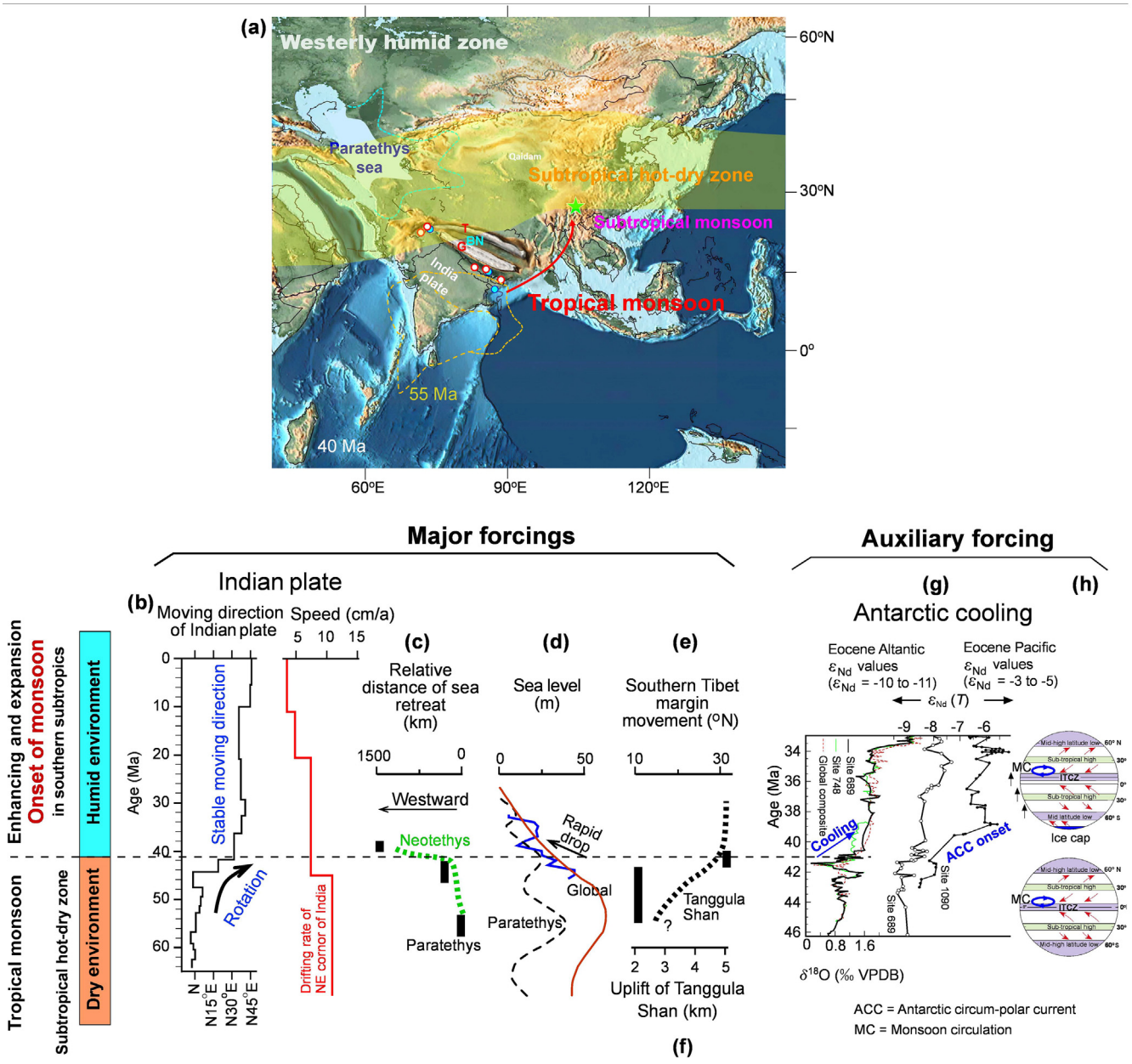

Fig. 4. Diagram showing the concurrence or coupling of the major forcings responses for enhancement and expansion of the tropical IM to the southern subtropics at ~41 Ma. (a) Paleogeography and paleoclimatic pattern of Asia at 40 Ma showing a full merging of Indian plate with Asian continent at ~41 Ma. Note the tropical monsoon was confined below 20°N. Red and light blue circles indicate the youngest marine stratigraphy at ~41 and 35 Ma, respectively (Fig. S9 online for details). G, T and BN indicate the Gangdese Shan, Tanggula Shan and the Bangong-Nujiang lowland between the Gangdese Shan and the Tanggula Shan. Yellow (dotted) broken line shows the (Great) Indian plate at 55 Ma. Light blue broken line indicates the range of the Paratethys sea at 42–47 Ma (compiled from Refs. [39–42]). Green star marks the location of the studied region. Paleogeography was modified from Ref. [38] for the latest updated topographic revision for the Tibetan region [43] and the sea boundary revision for the Paratethys sea at ~40–39 Ma [39,40]. (b) Variations of moving speed and direction of the Indian plate during the Cenozoic [36]. (c), (d) Westward retreat and sea level drop of the Neotethys and Paratethys seas (calculated from Fig. S9 online and its references). Global sea level falls from Ref. [44] (brown solid line) and in detail from Ref. [45] (blue solid line) are also plotted in (d) for comparison. (e) Northward movement of the southern margin of the Tibetan Plateau, calibrated for the reference point (29°N, 88°E) in the Gangdese Shan [46] from Refs. [47,48]. (f) Uplift of the Tanggula Shan, complied from Refs. [15,49,50]. (g) Cooling and ephemeral onset of the Antarctic ice sheet [51–53]. (h) Northward migration of global planetary circulation zones driven by the Antarctic ice sheet expansion.

thickening and magmatic and volcanic addition should have further lifted the Gangdese Shan. The existence of the elevated Gangdese Shan served as the southern boundary of the TP before the Miocene uplift of the Himalayas. It has been proposed that the IM precipitation is particularly sensitive to the Himalayas which can intensify the IM via its orographic and thermal role [4]. We argue before uplift of the Himalayas, the Gangdese Shan has served as a similar role to the Miocene Himalayas as a forcing for the IM.

Third, recent detailed paleomagnetism of the Linzizong volcanic rocks reveals a fast and large scale northward movement of the Gangdese Shan around 41 Ma from about 10.5° + 4.3°/−4.0°N at 55–43 Ma or 20.8° + 4.1°/−3.7°N at 54–47 Ma to 31.5°+5.1°/−4.5°N at 43–40 Ma [47,48,57], calibrated for the reference point (29°N, 88°E) in the Gangdese Shan [46] (Fig. 4e). Even if there is large uncertainties associated with paleomagnetic reconstruction of paleolatitudes [58], this fast latitudinal change is generally consistent with the fact that the southern margin of the Tibetan Plateau was indented and pushed to move northwards in a great deal to absorb at least 1000 km indentation by the Indian plate, especially at the time of "full-merging" of the India and Asia

continents. Because the Gangdese Shan acted locally as a barrier for monsoon moisture input, we argued that a fast northward movement of the high Gangdese Shan at ~41 Ma would have allowed the northward expansion of the monsoon moisture at that time. This is also supported by some recent numerical modeling [59,60].

Fourth, the pulse uplift of the Tanggula Shan in the central TP at ~43–40 Ma [49,61,62] is also likely a response to the full merging of the Indian-Asian continents and might serve also as a forcing factor to enhance the IM at ~41 Ma due to its mechanical and thermal functions akin to those of the Himalaya [4]. Although the southern-central TP was recently demonstrated to develop a broad Bangong-Nujiang lowland between the Gangdese Shan and the Tanggula Shan (Mts.) [15,43], the Tanggula Shan had also attained great crust thickening and partial melting and volcanism at ~45–38 Ma [61,63,64], followed by a phase of rapid deformation and uplift at ~43–40 Ma [49,61,62], probably having attained its present elevation in the late Eocene [15,49,50] (Fig. 4f). This is probably due to its location in the previously-existed weakened suture and orogenic belt, or subduction of the northern Lhasa block beneath the Qiangtang block [62], or magmatic addition or a combination of the above [43]. Thus, the thermal role of the Tanggula Shan can attract the tropical IM moisture to flow into the broad Bangong-Nujiang lowland and mechanically hit the Tanggula Shan to rain and release latent heating, which in turn will enhance the IM. Uplift of the central TP has been numerically modelled to enhance the IM [60].

As partially an eastern extension of the Tanggula Shan, the observation that the NW Yunnan was uplifted to near its elevation (~2.6 km) by the latest ~40 Ma [65] may also contribute to enhance the dry to wet shift in Yunnan through raining and thermal effects.

Fifth, the ephemeral Antarctic glaciation and global cooling at ~41 Ma [51,52], driven by the initial Antarctic Circum-polar Current (ACC) and related enhanced ocean productivity caused by the initial opening of the Drake Passage between South America and Antarctic at that time [53], might add another force to drive all global planetary climate zones migrating northwards and thus enhance the Asian monsoon circulation to expand to Yunnan at that time (Fig. 4g, h). Such thinking was proposed for the late or modern monsoon enhancements [1,66].

Our results do not support that CO_2 has played a paramount role in determining the IM intensity in the Eocene, as suggested by some studies [14], because CO_2 was higher during the early Eocene than the later Eocene [67]. Instead, we observed IM intensification at the low CO_2 late Eocene. The less strong IM during the high CO_2 early Eocene suggests that tectonics was likely the dominant forcing factor for Asian monsoon evolution, consistent with a similar conclusion made regarding EAM based on numerical model integration [43].

In summary, the paleoclimatic and paleoenvironmental records from Yunnan provide a comprehensive understanding of the IM variations for the first time. The records reveal that the modern alike IM did not exist in the subtropical zone until after 41 Ma. This new finding on the onset of the IM in the southern subtropics at 41 Ma requires a revision of our current understanding of the first-order controlling factors of the IM. The concurrence or coupling of combined factors (greatly enlarged land area, thus increased land-sea contrast due to closure of the Neotethys sea and retreat of the Paratethys sea with fast global sea drop and Antarctic cooling, fast northward movement of the southern margin of the TP, lifted Gangdese Shan, and rapid uplift of the central TP) might have collectively resulted in the greatly enhanced tropical IM and its northward expansion to the southern subtropics. Our results suggest a less important role of CO_2 to the IM and have significant implications for understanding future IM variations. Although we listed a few potential mechanisms for the observed fast dry-wet transition in Yunnan at 41 Ma, we could not pin down the ultimate mechanisms for this event. However, some insights can be gained from rapid climatic transitions like EOT (Eocene–Oligocene transition) [68,69] and MMCT (middle Miocene climate transition) [70], in which special orbital configuration helped the climatic system to cross some tipping point within the context of slow paleoceanography or tectonic processes. Therefore, we infer that the fast nature observed here would likely require a similar mechanism. In future, numerical modelling is needed to pin down the exact mechanisms for this environmental shift in the Eocene. We anticipate that one of the above mentioned mechanisms, or a combination of them, under the influence of orbital parameter changes and long term CO_2 decrease, would be able to explain the observed likely most dramatic Asian environmental shift in the Eocene.

Conflict of interest

The authors declare that they have no conflict of interest.

Acknowledgments

This work was co-supported by the Strategic Priority Research Program of Chinese Academy of Sciences (XDA20070201), the National Natural Science Foundation of China Basic Science Center for Tibetan Plateau Earth System (41988101-1), the National Natural Science Foundation of China (41620104002), and the Second Tibetan Plateau Scientific Expedition and Research Program (2019QZKK0707). We thank Robert A. Spicer for his constructive comments and revisions for the early drafts and three anonymous reviewers for their valuable comments and suggestions that helped improving the quality of the manuscript. Thanks also due to Yan Bai, Yunfa Miao, Xijun Ni, Qingquan Meng, Dangpeng Xi, Miaomiao Shen, Ying Tian, Bingshuai Li, Shuang Lü, Rongsheng Yang, Ziqiang Mao, Liye Yang, Chihao Chen, Yahui Fang, Shoujie Gao, Jiuyi Wang, Yi Chen, Jiwei Yang, and Song Wu for their laboratory and fieldwork assistances.

Author contributions

Xiaomin Fang and Maodu Yan designed and wrote the manuscript. Junsheng Nie contributed to the discussion of scientific questions and the revision of the manuscript. Weilin Zhang, Wenxia Han, Fuli Wu, Chunhui Song, Tao Zhang, Jinbo Zan and Yongpeng Yang contributed to the sampling of the section and analyzed the lithofacies, salinity, redness and pollens.

Appendix A. Supplementary materials

Supplementary materials to this article can be found online at https://doi.org/10.1016/j.scib.2021.07.023.

References

[1] Wang B. The Asian monsoon. New York: Springer; 2006. p. 1–836.
[2] Kitoh A, Endo H, Krishna Kumar K, et al. Monsoons in achanging world: a regional perspective in a global context. J Geophys Res Atmos 2013;118:3053–65.
[3] Johnson KR. Palaeoclimate: long-distance relationship. Nat Geosci 2011;4:426–7.
[4] Boos WR, Kuang Z. Dominant control of the South Asian monsoon by orographic insulation versus plateau heating. Nature 2010;463:218–22.
[5] Wu GX, Liu YM, He B, et al. Thermal controls on the Asian summer monsoon. Sci Rep 2012;2:1–7.
[6] Liu X, Dong B, Yin ZY, et al. Continental drift, plateau uplift, and evolutions of monsoon and arid regions in Asia, Africa, and Australia during the Cenozoic. Sci China Earth Sci 2019;62:1053–75.

[7] Clemens SC, Prell WL, Sun Y. Orbital-scale timing and mechanisms driving Late Pleistocene Indo-Asian summer monsoons: reinterpreting cave speleothem $\delta^{18}O$. Paleoceanography 2010;25:PA4207.
[8] Molnar P, England P, Martinod J. Mantle dynamics, uplift of the Tibetan Plateau, and the Indian monsoon. Rev Geophys 1993;31:357–96.
[9] Kutzbach JE, Prell WL, Ruddiman WF. Sensitivity of Eurasian climate to surface uplift of the Tibetan Plateau. J Geol 1993;101:177–90.
[10] Clift PD, Hodges KV, Heslop D, et al. Correlation of Himalayan exhumation rates and Asian monsoon intensity. Nat Geosci 2008;1:875–80.
[11] Huber M, Goldner A. Eocene monsoons. J Asian Earth Sci 2012;44:3–23.
[12] Quan C, Liu Z, Utescher T, et al. Revisiting the Paleogene climate pattern of East Asia: a synthetic review. Earth-Sci Rev 2014;139:213–30.
[13] Shukla A, Mehrotra RC, Spicer RA, et al. Cool equatorial terrestrial temperatures and the South Asian monsoon in the Early Eocene: evidence from the Gurha Mine, Rajasthan, India. Palaeogeogr Palaeoclimatol Palaeoecol 2014;412:187–98.
[14] Licht A, van Cappelle M, Abels HA, et al. Asian monsoons in a late Eocene greenhouse world. Nature 2014;513:501–6.
[15] Ding L, Xu Q, Yue Y, et al. The Andean-type Gangdese Mountains: Paleoelevation record from the Paleocene-Eocene Linzhou Basin. Earth Planet Sci Lett 2014;392:250–64.
[16] An Z, Sun YB, Chang H, et al. Late Cenozoic climate change in Asia: loess, monsoon and monsoon-arid environment evolution, 16. Dordrecht: Springer; 2014. p. 1–582.
[17] Spicer RA, Yang J, Herman AB, et al. Asian Eocene monsoons as revealed by leaf architectural signatures. Earth Planet Sci Lett 2016;449:61–8.
[18] Spicer R, Yang J, Herman A, et al. Paleogene monsoons across India and South China: drivers of biotic change. Gondwana Res 2017;49:350–63.
[19] Xiong Z, Ding L, Spicer RA, et al. The early Eocene Rise of the Gonjo Basin, SE Tibet: from low desert to high forest. Earth Planet Sci Lett 2020;543:116312.
[20] Valdes PJ, Ding L, Farnsworth A, et al. Comment on "Revised paleoaltimetry data show low Tibetan Plateau elevation during the Eocene". Science 2019;365:eaax8990.
[21] Farnsworth A, Lunt DJ, Robinson SA, et al. Past East Asian monsoon evolution controlled by paleogeography, not CO_2. Sci Adv 2019;5:eaax1697.
[22] Guo ZT, Sun B, Zhang ZS, et al. A major reorganization of Asian climate by the early Miocene. Clim Past 2008;4:153–74.
[23] Bureau of Geology and Mineral Sources of Yunnan Province. Regional geology of Yunnan Province. Beijing: Geological Publishing House; 1990.
[24] Ni X, Li Q, Li L, et al. Oligocene primates from China reveal divergence between African and Asian primate evolution. Science 2016;352:673–7.
[25] Gourbet L, Leloup PH, Paquette J-L, et al. Reappraisal of the Jianchuan Cenozoic basin stratigraphy and its implications on the SE Tibetan Plateau evolution. Tectonophysics 2017;700-701:162–79.
[26] Linnemann U, Su T, Kunzmann L, et al. New U-Pb dates show a Paleogene origin for the modern Asian biodiversity hot spots. Geology 2017;46:3–6.
[27] Gradstein FM, Ogg JG, Schmitz MD, et al. The geologic time scale 2012. Amsterdam: Elsevier; 2012.
[28] Talbot MR, Kelts K. Lacustrine Basin exploration: case studies and modern analogs, 50. Tulsa: American Association of Petroleum Geologists; 1990. p. 99–112.
[29] Wang BY, Zhang YP. New finds of fossils from Paleogene of Qujing, Yunnan. Vertebr Palasiat 1983;21:119–28 (in Chinese).
[30] Tong YS, Zheng SH, Qiu ZD. Cenozoic mammal ages of China. Vertebr Palasiat 1995;33:307–14.
[31] Schwertmann U. Transformation of hematite to goethite in Soils. Nature 1971;232:624–5.
[32] Zhang YG, Ji JF, Balsam WL, et al. High resolution hematite and goethite records from ODP 1143, South China Sea: co-evolution of monsoonal precipitation and El Niño over the past 600000 years. Earth Planet Sci Lett 2007;264:136–50.
[33] Tan LC, Cai YJ, An ZS, et al. Decreasing monsoon precipitation in southwest China during the last 240 years associated with the warming of tropical ocean. Clim Dynam 2017;48:1769–78.
[34] Wan GJ, Bai ZG, Qing H, et al. Geochemical records in recent sediments of Lake Erhai: implications for environmental changes in a low latitude-high altitude lake in southwest China. J Asian Earth Sci 2003;21:489–502.
[35] Zhang HC. A comment on Lai et al. (2014) concerning the origin of the Shell Bar section from the Qaidam Basin, NE Tibetan Plateau: lake formation versus river channel deposit, and ^{14}C versus OSL dates. J Paleolimnol 2015;53:321–334.
[36] Molnar P, Stock JM. Slowing of India's convergence with Eurasia since 20 Ma and its implications for Tibetan mantle dynamics. Tectonics 2009;28:1–11.
[37] Zheng Y, Wu F. The timing of continental collision between India and Asia. Sci Bull 2018;63:1649–54.
[38] Scotese CR, Wright N. Paleomap Paleodigital Elevation Models (PaleoDEMS) for the Phanerozoic Paleomap Project. 2018; https://www.earthbyte.org/paleodem-resource-scotese-and-wright-2018/.
[39] Bosboom RE, Dupont-Nivet G, Houben AJP, et al. Late Eocene sea retreat from the Tarim Basin (west China) and concomitant Asian paleoenvironmental change. Palaeogeogr Palaeoclimatol Palaeoecol 2011;299:385–98.
[40] Sun J, Windley BF, Zhang Z, et al. Diachronous seawater retreat from the southwestern margin of the Tarim Basin in the late Eocene. J Asian Earth Sci 2016;116:222–31.
[41] Ramstein G, Fluteau F, Besse J, et al. Effect of orogeny, plate motion and land-sea distribution on Eurasian climate change over the past 30 million years. Nature 1997;386:788–95.
[42] Zhongshi Z, Wang H, Guo ZT, et al. What triggers the transition of palaeoenvironmental patterns in China, the Tibetan Plateau uplift or the Paratethys Sea retreat? Palaeogeogr Palaeoclimatol Palaeoecol 2007;245:317–31.
[43] Fang XM, Dupont-Nivet G, Wang CS, et al. Revised chronology of central Tibetan uplift (Lunpola Basin). Sci Adv 2020;6:eaba7298.
[44] Miller KG, Kominz MA, Browning JV, et al. The Phanerozoic record of global sea-level change. Science 2005;310:1293–8.
[45] Cramer BS, Miller KG, Barrett PJ, et al. Late Cretaceous–Neogene trends in deep ocean temperature and continental ice volume: reconciling records of benthic foraminiferal geochemistry ($\delta^{18}O$ and Mg/Ca) with sea level history. J Geophys Res 2011;116:C12023.
[46] Zhang DW, Yan MD. Paleomagnetic constraints on the onset of India-Eurasia collosion: a synthesis. Geol Rev 2019;25:1251–68 (in Chinese).
[47] Tan X, Gilder S, Kodama KP, et al. New paleomagnetic results from the Lhasa block: revised estimation of latitudinal shortening across Tibet and implications for dating the India-Asia collision. Earth Planet Sci Lett 2010;293:396–404.
[48] Chen JS, Huang B, Yi Z, et al. Paleomagnetic and $^{40}Ar/^{39}Ar$ geochronologic results from the Linzizong Group, Linzhou Basin, Lhasa Terrane, Tibet: implications to Paleogene paleolatitude and onset of the India-Asia collision. J Asian Earth Sci 2014;96:162–77.
[49] Wang CS, Zhao XX, Liu ZF, et al. Constraints on early uplift history of the Tibetan Plateau. Proc Natl Acad Sci USA 2008;105:4987–92.
[50] Lin J, Dai J, Zhuang GS, et al. Late Eocene-Oligocene high relief paleotopography in the north central Tibetan Plateau: insights from detrital zircon U-Pb geochronology and leaf wax hydrogen isotope studies. Tectonics 2020;39:e2019TC005815.
[51] Tripati A, Backman J, Elderfield H, et al. Eocene bipolar glaciation associated with global carbon cycle changes. Nature 2005;436:341–6.
[52] Zachos J, Pagani M, Sloan L, et al. Trends, rhythms, and aberrations in global climate 65 Ma to present. Science 2001;292:686–93.
[53] Scher H, Martin E. Timing and climatic consequences of the opening of Drake Passage. Science 2006;312:428–430.
[54] Mo X, Hou Z, Niu Y, et al. Mantle contributions to crustal thickening during continental collision: evidence from Cenozoic igneous rocks in southern Tibet. Lithos 2007;96:225–42.
[55] Ji WQ, Wu FY, Chung SL, et al. Zircon U-Pb chronology and Hf isotopic constraints on the petrogenesis of Gangdese batholiths, southern Tibet. Chem Geol 2009;262:229–45.
[56] Jiang Z-Q, Wang Q, Wyman DA, et al. Transition fromoceanic to continental lithosphere subduction in southern Tibet: evidence from the Late Cretaceous-Early Oligocene (~91–30 Ma) intrusive rocks in the Chanang-Zedong area, southern Gangdese. Lithos 2014;196-197:213–31.
[57] Dupont-Nivet G, Lippert PC, van Hinsbergen DJJ, et al. Palaeolatitude and age of the Indo-Asia collision: palaeomagnetic constraints. Geophys J Int 2010;182:1189–98.
[58] Rowley DB. Comparing paleomagnetic study means with apparent wander paths: a case study and paleomagnetic test of the Greater India versus Greater Indian Basin hypotheses. Tectonics 2019;38:722–40.
[59] Zhang R, Jiang D, Ramstein G, et al. Changes in Tibetan Plateau latitude as an important factor for understanding East Asian climate since the Eocene: a modeling study. Earth Planet Sci Lett 2018;484:295–308.
[60] Zhu C, Meng J, Hu Y, et al. East-Central Asian climate evolved with the northward migration of the high proto-Tibetan Plateau. Geophys Res Lett 2019;46:8397–406.
[61] Wang Q, Wyman DA, Xu J, et al. Eocene melting of subducting continental crust and early uplifting of central Tibet: evidence from central-western Qiangtang high-K calc-alkaline andesites, dacites and rhyolites. Earth Planet Sci Lett 2008;272:158–71.
[62] Kapp P, Yin A, Harrison TM, et al. Cretaceous-Tertiary shortening, basin development, and volcanism in central Tibet. Geol Soc Am Bull 2005;117:865–78.
[63] Chung S-L, Chu M-F, Zhang Y, et al. Tibetan tectonic evolution inferred from spatial and temporal variations in post-collisional magmatism. Earth Sci Rev 2005;68:173–96.
[64] Ding L, Kapp P, Yue Y, et al. Postcollisional calc-alkaline lavas and xenoliths from the southern Qiangtang terrane, central Tibet. Earth Planet Sci Lett 2007;254:28–38.

[65] Li S, Currie BS, Rowley DB, et al. Cenozoic paleoaltimetry of the SE margin of the Tibetan Plateau: constraints on the tectonic evolution of the region. Earth Planet Sci Lett 2015;432:415–24.
[66] An Z, Clemens SC, Shen J, et al. Glacial-interglacial Indian summer monsoon dynamics. Science 2011;333:719–723.
[67] Beerling DJ, Royer DL. Convergent Cenozoic CO_2 history. Nat Geosci 2011;4:418–20.
[68] Ladant J-B, Donnadieu Y, Lefebvre V, et al. The respective role of atmospheric carbon dioxide and orbital parameters on ice sheet evolution at the Eocene-Oligocene transition. Paleoceanography 2014;29:810–23.
[69] Ao H, Dupont-Nivet G, Rohling EJ, et al. Orbital climate variability on the northeastern Tibetan Plateau across the Eocene-Oligocene transition. Nat Commun 2020;11:5249.
[70] Shevenell AE, Kennett JP, Lea DW. Middle Miocene southern ocean cooling and Antarctic cryosphere expansion. Science 2004;305:1766–70.

Xiaomin Fang is a professor of the Institute of Tibetan Plateau Research, Chinese Academy of Sciences. His research focuses on the uplift of the Tibetan Plateau and environmental change.